CrystEngComm

Accepted Manuscript

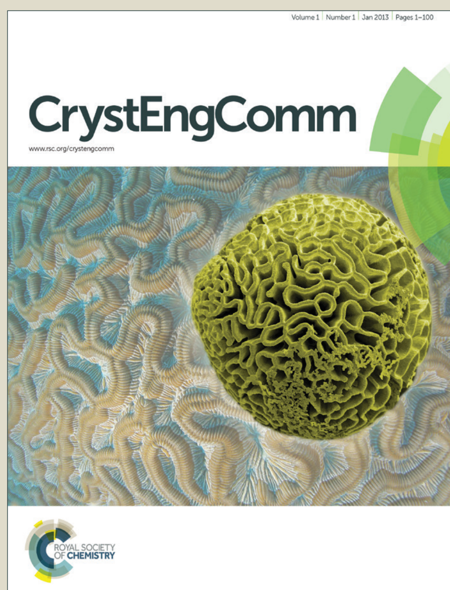

This is an *Accepted Manuscript*, which has been through the Royal Society of Chemistry peer review process and has been accepted for publication.

Accepted Manuscripts are published online shortly after acceptance, before technical editing, formatting and proof reading. Using this free service, authors can make their results available to the community, in citable form, before we publish the edited article. We will replace this *Accepted Manuscript* with the edited and formatted *Advance Article* as soon as it is available.

You can find more information about *Accepted Manuscripts* in the Information for Authors.

Please note that technical editing may introduce minor changes to the text and/or graphics, which may alter content. The journal's standard Terms & Conditions and the Ethical guidelines still apply. In no event shall the Royal Society of Chemistry be held responsible for any errors or omissions in this *Accepted Manuscript* or any consequences arising from the use of any information it contains.

ROYAL SOCIETY OF CHEMISTRY

www.rsc.org/crystengcomm

Effect of Catalyst Shape on Etching Orientation in Metal-assisted Chemical Etching of Silicon

Weiwei Xia*, Jun Zhu, Haibo Wang, Xianghua Zeng*

College of Physics Science and Technology & Institute of Optoelectronic Technology ,Yangzhou University, Yangzhou 225002, P.R. China

Abstract:

Silicon nanowires with vertical, slanting and zigzag architectures have been fabricated by metal-assisted chemical etching of silicon wafers (n-Si(100), n-Si(111) and n-Si(110)). Two types of zigzag SiNWs with various turning angles (125° and 150°) via metal-assisted chemical etching using non-Si(100) wafers were obtained. The observations reveal that the etching direction of non-Si(100) wafers depends on the shape of the deposited metal catalyst. A proposal mechanism integrally with longitudinal and lateral etching has been developed to explain the etching behaviors.

* *Corresponding authors. Email: wwxia@yzu.edu.cn and xhzeng@yzu.edu.cn*

CrystEngComm Accepted Manuscript

I. INTRODUCTION

Over the past years, silicon nanowires (SiNWs) have attracted considerable attention owing to their promising applications in broad areas ranging from photovoltaics[1-3], field-effect transistors (FETs)[4,5] and battery electrodes[6] to biosensors[7]. SiNWs are produced by various methods such as laser ablation[8], thermal evaporation[9] and chemical vapor deposition[10]. Among those fabrication methods, metal-assisted chemical etching (MACE) method has recently attracted considerable attention as a promising alternative SiNW fabrication compared to the aforementioned techniques for several reasons. First, MACE method is very simple and cheap, and can be used to fabricate large-scale SiNWs. Second, MACE method can control easily various parameters (e.g., diameter, length, crystallographic orientation, and density[11-13]) of SiNWs by adjusting the etchant concentration and the etching time. In this approach, noble metals (e.g., Ag, Au, etc.) on a silicon wafer are used as catalysts in the chemical etching of silicon with an aqueous solution containing HF and an oxidant (H_2O_2 or metal salts, such as $AgNO_3$, $KAuCl_4$, $Fe(NO_3)_3$)[14-18].

The morphologies and crystallographic orientations[19-20], as much as the intrinsic properties, play a decisive role in their applications, such as vertical-SiNWs-based FETs[4,5] and slanting-SiNWs-based solar cells[21]. However, the control of the orientations of the SiNWs to substrate is still a big challenge. Recently, the wafer-scale vertically-aligned, slantingly-aligned and zigzag-shaped SiNWs could be fabricated by adjusting the etching conditions and using various Si substrates with different orientations and doping levels[22-28]. It was demonstrated that the orientation of SiNWs was affected by the geometric characteristics of the catalyst and the relative concentrations of the oxidant and HF. More recently, Huang et al[23]. reported a systematic study of the catalyst-morphology dependence of metal-assisted etching of Si(110) wafers. In the case of isolated metal particles or relatively small patches of metal films with perforating nanoholes, the etching direction of Si(110) substrates was predominantly along <100> direction. In contrast, the etching direction was confined to the vertical <$\bar{1}\bar{1}0$> direction, when lateral size of the catalytic metal mesh was sufficiently large. The SiNWs

CrystEngComm Accepted Manuscript

1 etched on Si(111) substrates appear to have more complicated etching direction than those on Si(100) and Si
2 (110) substrates. At the same time, Chen et al. found etching to proceed in the vertical <111> direction on a
3 (111)-oriented Si substrate with a low oxidant ($AgNO_3$) concentration at low temperature. In contrast, when
4 the etching was carried out with a higher oxidant concentration at a higher temperature, three types of
5 zigzag-shaped SiNWs with different turning angles can be simultaneously formed[22]. They explained the
6 change in angle during MACE using an argument based on the different potential barriers, which the Ag
7 catalysts should overcome to change etching directions. However, the exact mechanism responsible for the
8 switch in etching directions is problematic. In order to better understand the dependence of
9 crystallographic-orientation in etching process, we systematically investigate the etching behavior of different
10 Si wafers, and then propose a mechanism considering the longitudinal and lateral etching to explain the
11 etching behavior.

12 II. EXPERIMENTAL PROCEDURE

13 Three types of Si wafers, which were n- (100) (ρ: 0.01-0.018 $\Omega \cdot cm$), n- (110) (ρ: 1-10 $\Omega \cdot cm$), and
14 n- (111) (ρ: 0.007-0.02 $\Omega \cdot cm$) have been used as starting wafers. Prior to the etching process, Si wafers
15 were ultrasonically cleaned in acetone, ethanol and then de-ionized water at room temperature all for 15 min,
16 respectively. Then the wafers were immersed in a 3:1 mixture of 97% H_2SO_4 and 30% H_2O_2 for 30 min to
17 remove organic residues and heavy metals. After each cleaning step, the wafers were rinsed with de-ionized
18 water followed by dipping in 10% hydrofluoric acid (HF) solution to remove any surface oxides. Our
19 chemical etching method to produce SiNW arrays is based on a two-step metal-assisted chemical etching
20 method**.** In the first step, Ag nanoparticles (AgNPs) were deposited on silicon wafers surfaces by immersing
21 the wafers in aqueous solution of silver nitrate ($AgNO_3$) and HF for 1 min at room temperature. Four plating
22 solutions were used in our experiments, which were solution I ([$AgNO_3$]=0.005 M, [HF]=4.8 M), solution II
23 ([$AgNO_3$]=0.01 M, [HF]=4.8 M), solution III ([$AgNO_3$]=0.15 M, [HF]=4.8 M), solution IV ([$AgNO_3$]=0.02

CrystEngComm Accepted Manuscript

1 M, [HF]=4.8 M). The morphology of the forming Ag nanoparticles strongly depend on the concentration of $AgNO_3$. In the second step, silicon wafers covered with AgNPs of different morphology were immersed in the etching solution containing 4.8 M HF and 0.7 M H_2O_2 for 30 min at room temperature. Finally the samples after the etching procedures were thoroughly rinsed several times in deionized water and dried naturally at room temperature.

Cross-sectional views of the samples were observed by SEM (Hitachi S-4800) and elemental analysis was analyzed by energy dispersive X-ray spectroscopy (EDS). High resolution transmission electron microscopy (HRTEM) images were captured on a Tecanai G2 F30 S-Twin microscope with at an accelerating voltage of 300 kV.

III. RESULTS AND DISCUSSION

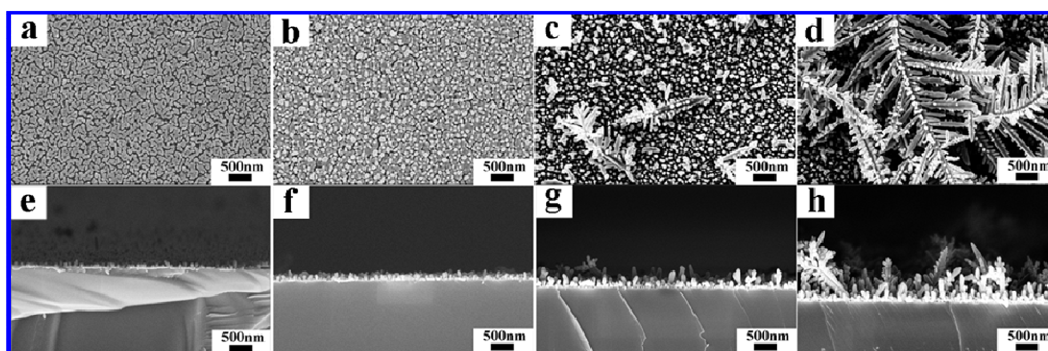

Figure 1. Plan view and Cross-sectional SEM images of silver particles loaded on n-type (111) substrate via electroless plating with the deposition time of 60 s. (a), (e) in solution I; (b), (f) in solution II; (c), (g) in solution III; (d), (h) in solution IV.

The influence of the $AgNO_3$ concentration on the morphology of Ag catalysts deposited on Si wafers was systematically investigated. Figures 1(a)-(d) are SEM top-view images of cleaned Si wafers which were immersed in the plating solution with different $AgNO_3$ concentrations for 60 s, where the concentration of $AgNO_3$ is increased from 0.005 M to 0.02 M. Figure 1(a) displays a plan view SEM image of Si (111) wafer immersed in the aqueous solution with 4.8 M HF-0.005 M $AgNO_3$. It clearly reveals that the silicon substrate was covered with many AgNPs. When the concentration of $AgNO_3$ increased from 0.005 M to 0.1 M, the morphology of AgNPs did not change remarkably. Further increasing the concentration of $AgNO_3$, as shown

CrystEngComm Accepted Manuscript

in figure 1 (c) and (d), a large amount of nanoclusters and tree-like silver dendrites appear on these Si substrates. Figures 1(e)-(h) show corresponding cross-sectional images of these Si substrates with Ag catalysts fabricated with different $AgNO_3$ concentrations. The shapes of Ag catalysts change dramatically with the $AgNO_3$ concentration. When the concentration of $AgNO_3$ is 0.005 M, Ag catalysts appear in a sphere shape with uniform diameter (~50 nm). However, a few rod- and antler-like Ag structures appear on Si wafers when the $AgNO_3$ concentration is increased to 0.01 M. Further increasing the concentration of $AgNO_3$, a large number of silver dendrites form on the Si substrate. When the $AgNO_3$ concentration is increased to 0.02 M, the mean length of Ag nanorod is about 750 nm as shown in figure 1(h).

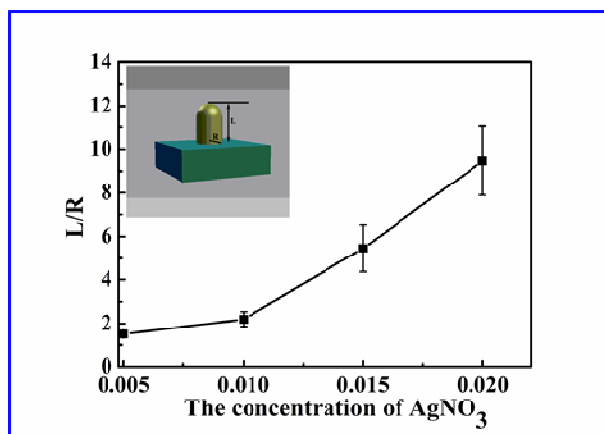

Figure 2. The relationship between the L/R ratio of Ag nanostructure and the $AgNO_3$ concentration.

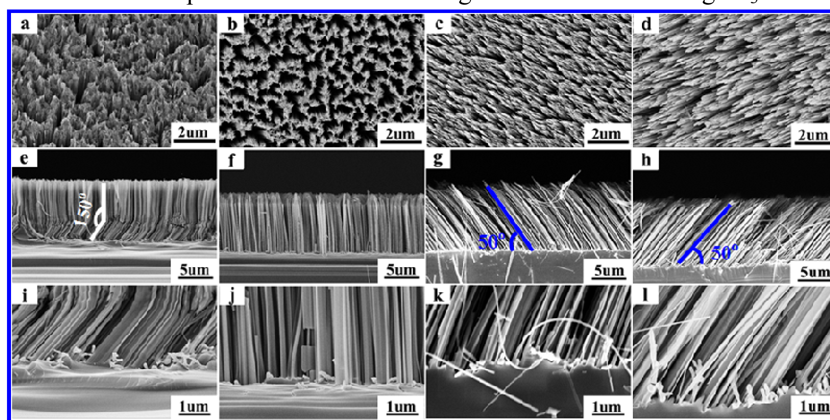

Figure 3. SEM images of SiNW arrays on n-type Si(111) substrate:(a), (b), (c), (d) planar images with no tilt angle; (e), (f), (g), (h) corresponding cross-sectional images; (i), (j), (k), (l) enlarged cross-sectional images of the bottom of the arrays. Silver catalysts were obtained solution I (a, e, i) , solution II (b, f, j), solution III (c, g, k) and solution IV (d, h, l).

In order to get quantitative information of the Ag catalyst formed with different $AgNO_3$ concentrations,

CrystEngComm Accepted Manuscript

1 the length, radius and (L/R) ratio of Ag structures have been measured and calculated, and the results are
2 shown in figure 2. It clearly shows that the average L/R ratio of Ag structure is approximately proportional to
3 the $AgNO_3$ concentration.

4 The electrochemical etching of Si(111) wafers appears to be more complicated than that of Si(100) and
5 Si(110) wafers. The anisotropic etching behavior of Si (111) wafers remains confusing because <100> is
6 usually thought to be the preferred etching direction[22]. Figure 3. shows the planar and cross section images of
7 the as-fabricated SiNW arrays on Si(111) substrates, which were etched in the aqueous solution of 0.7 M
8 H_2O_2 and 4.8 M HF for 30 min at room temperature. Wafer-scale zigzag-shaped, well vertically-aligned and
9 slantingly-aligned SiNWs have been fabricated. The turning angle of wafer-scale zigzag-shaped SiNWs was
10 150° (Figure 3e and i) implying that the etching direction changes from one <111> to another direction in the
11 case of minimum L/R ratio of AgNPs,. As the L/R ratio of AgNPs increases to 2.19, the etching occurred
12 along the vertical direction of the substrate, which is <111> direction, leaving vertically aligned SiNW array
13 (Figure 3f and j). As the L/R ratio of AgNPs further increases to 5.5 and 9.5, the etching occures in inclined
14 direction. Uniform slantingly-aligned SiNW arrays with the angle of 50° relative to the substrate were
15 formed as shown in Figure 3(g) and (h).

16 HRTEM investigations were carried out to observe the microstructures of the three types of SiNWs.
17 Figure 4 shows TEM and HRTEM images of a typical single zigzag SiNW with a turning angle of 150°.
18 HRTEM images of two selected segments of the single zigzag-shaped SiNW are displayed in figures 4(b)
19 and (c). The space distance is 3.134 Å, which is consistent with the lattice-plane (111) of crystalline Si. The
20 FFT pattern shown in figure 4 confirms the etching direction changes from <111> to <113>. It can be
21 concluded that the etching direction is initially along a straight <111> orientation down to several
22 micrometers and then changes into the more energetically favorable <113> direction.

CrystEngComm Accepted Manuscript

1 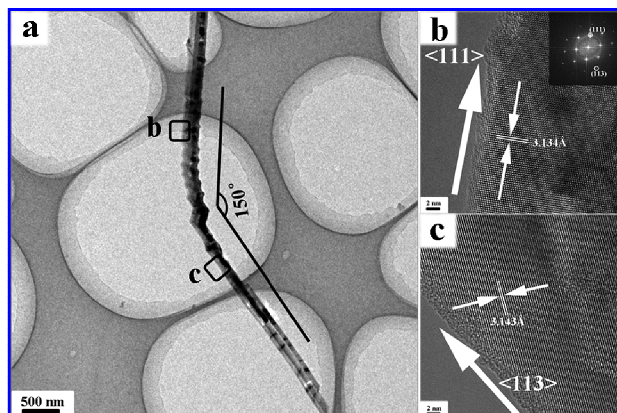

2 Figure 4. TEM and HRTEM characterizations of an individual SiNW fabricated by etching Si(111) wafers in the aqueous
3 solution of 0.7 M H_2O_2 and 4.8 M HF for 30 min at room temperature, and Ag catalysts were synthesized in aqueous solution I.
4 Low-magnification image (a) and high-magnification bright-field images of the zigzag-shaped SiNW (b) above and (c) below
5 the etching direction transition. The inset of (b) shows the corresponding Fast Fourier transform (FFT) patterns.

6 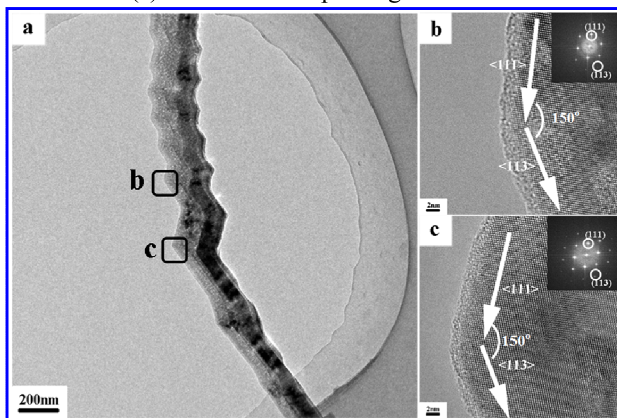

7 Figure 5. Enlarged TEM image (a) of an individual SiNW shown in figure 4(a), and HRTEM images (b) and (c) of parts b and
8 c marked in (a). The insets of (b) and (c) show the corresponding Fast Fourier transform (FFT) patterns of the HRTEM
9 imagesrespectively .

10 Figure 5 is the enlarged TEM image of an individual SiNW shown in figure 4(a). Saw-tooth facets have
11 been found at transition part of the zigzag-shaped SiNW, which implies that the etching direction shifts with
12 high frequency. Figures 5(b) and (c) are HRTEM images of the selected segments (parts a and b in figure 5(a))
13 of the saw-tooth structure. The lattice planes in HRTEM images and FFT patterns of the selected areas
14 confirm that the change of the etching direction alternates between <111> to <113> direction. The results
15 have been reported by Chen *et. al*. They believed that the etching direction switching from <111> to <113> is
16 due to perturbations (e.g caused by hydrogen bubbles) and the direction switching back to <111> is due to the
17 fact that <113> direction is not the energetically favorable etching direction. However, both <113> and <111>

CrystEngComm Accepted Manuscript

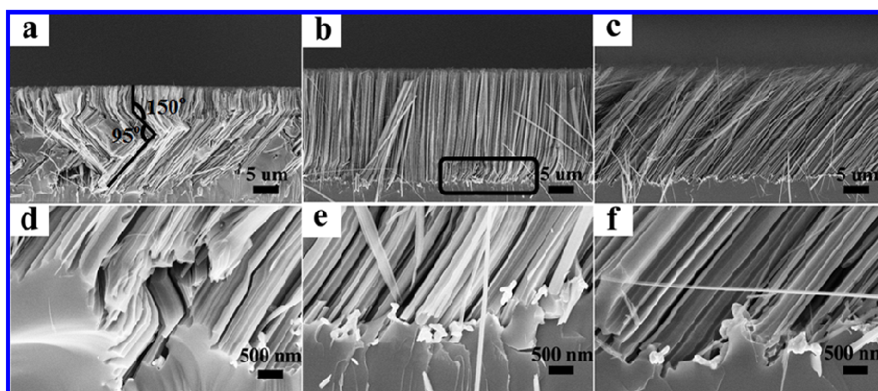

Figure 6.SEM images of SiNW arrays on n-type Si(111) substrate:(a), (b), (c) cross section images; (d), (e), (f) enlarged cross-sectional images of the bottom of the arrays. SiNWs were obtained in the aqueous solution of 0.7 M H_2O_2 and 4.8 M HF for 60 min at room temperature with different metallization aqueous solution: (a), (d) in solution I; (b), (e) in solution II; (c), (f) in solution IV. As discussed earlier, the angle between [111] and [113] is about 150°.The angle between [113] and [100] is calculated about 95°, where we can come to a conclusion that the etching direction switches again back to the lowest energy of <100> direction as etching time increases to 60 min.

have been identified as prevalent etching directions in the electrochemical etching of silicon[29]. In our case, it has also been found that the etching direction will finally switches to <100> direction as the etching time was increased to 60 min, which is shown in figure 6.

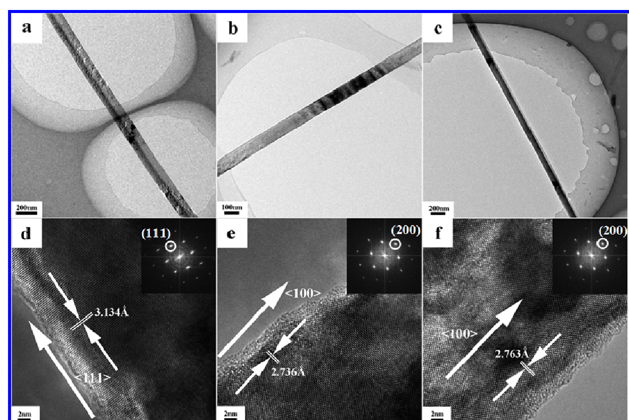

Figure 7. TEM and HRTEM images of an individual SiNW produced by MaCE of Si(111) in the aqueous solution of 0.7 M H_2O_2 and 4.8 M HF for 30 min at room temperature, in which Ag catalysts on Si wafers were obtained in different metallization aqueous solutions at room temperature for 1 min: (a), (d) solution II; (b), (e) solution III; (c), (f) solution IV.

Figure 7 shows TEM and HRTEM images of the as-fabricated single SiNW by etching n-(111) Si wafers for 30 min. Ag catalysts on Si wafers were obtained in different metallization aqueous solutions for 1 min. The SiNW etched by using the Ag catalysts formed in solution II is shown in figures 7(a) and (d). Figure 7(d) shows the lattice fringes with regular spacing of 3.134 Å, which is consistent with the inter-planar distance of

CrystEngComm Accepted Manuscript

(111) planes of crystalline Si. The well-resolved fringes confirm the single-crystal nature of the SiNW, which is in accordance with the corresponding FFT pattern shown in the inset of figure 7(d). The etching of Si wafer (111) starts initially in the <111> direction, but switches to the lower energy direction <100> finally when the etching time is long enough. The reason is that the <111> orientation is not the energetically favorable. (See figure 6). When Ag catalysts fabricated in 0.015M and 0.02M $AgNO_3$ solutions, HRTEM images of the corresponding etched SiNWs are shown in figures 7(e) and (f). The inter-planar spaces in figures 6(e) and (f) are 2.763 Å, matching with the (100) planes of crystalline Si. Owing to the lowest energy direction, <100> direction is the etching direction throughout the etching process.

The afore-mentioned results clearly indicate that the morphology of Ag catalyst obviously affects the etching direction of Si(111). It is generally accepted that the catalysts deposition from HF solution is a localized micro-electrochemical redox reaction process in which both anodic and cathodic processes occur simultaneously at the silicon surface and the Si below the areas covered with the metal catalyst were etched much faster than the bare surface, which indicates that the etching rate may depend on the area of the contact between the metal catalyst and substrate[18, 22]. Meanwhile, the contact between the metal catalyst and wafer includes not only the longitudinal direction but also the lateral direction as the etching process in its progress. According to the lattice structure of Si crystals, atoms on the (111) planes have three back bonds to the underneath atoms, whereas atoms on (100) planes have two back bonds. The back bonds on the (113) planes are found between the (111) planes and (100) planes[28,30-32]. We, therefore, propose a mechanism considering the combination of the surface state and longitudinal /lateral etching rate to explain the etching behavior. In the case of minimum L/R ratio of AgNPs in figures 1(a) and (e), initially, the longitudinal contact between catalyst and substrate is the main contact, which results in the dominant etching direction is longitudinal as shown in figure 3(e). Further increasing the etching time, the segment of metal catalysts that contacts with the sidewalls of SiNWs will progressively be oxidized into silver ion and deposit on the sidewalls of SiNWs,

CrystEngComm Accepted Manuscript

1 which will increases the average L/R ratio of AgNPs. And then, the lateral etching can not be ignored and the
2 etching process will be the integration of longitudinal and lateral etching, and the etching direction will switch
3 to the lower energy direction <113> and the zigzag structures formed as shown in figure 3(e). Since the
4 selection of energy is a gradual process, the etching direction changing from <111> to <113> can be
5 understood that the change of etching direction is also a process the selection process of energy. Among all
6 the direction, the <100> orientation is lowest energy direction and the <113> orientation is also not
7 energetically favorable. The etching direction will finally switch to the lowest energy of <100> direction as
8 etching time was increased and this suspicions is confirmed by figures 6(d).

9 The case of moderate L/R ratio of AgNPs as shown in figures 1(b) and (f). The longitudinal contact
10 between catalysts and substrate is also the main contact compared to the lateral contact between catalysts and
11 sidewalls of SiNWs , which results in the dominant etching direction is longitudinal as shown in figure 3(e).
12 However, the length of catalysts is much larger than the case of minimum L/R ratio of AgNPs, which lead to
13 the etching process can along the vertical direction of the substrate during the whole etching process (figure
14 3f). As increasing the etching time, the etching orientation will also switches to lower energy direction, which
15 is shown in figure 6 (e). Further increasing the average L/R ratio of catalysts as shown in figures 1c and 1d.
16 The contact between catalysts and substrate shows little difference in the lateral contact between catalysts and
17 sidewalls of SiNWs as increasing the L/R ratio of catalysts. In other words, the lateral etching rate was closed
18 to that of longitudinal etching, and the etching process will be the integration of longitudinal and lateral
19 etching at the initial etching stage process. In this case, slantingly-aligned SiNW arrays were obtained as
20 shown in figures 3(g) and (h).

21

CrystEngComm Accepted Manuscript

1 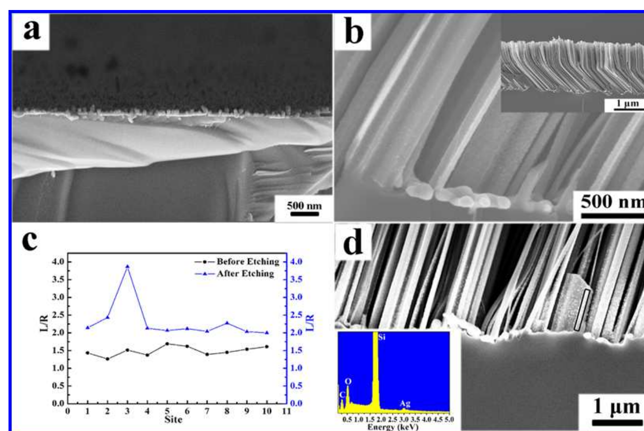

2 Figure 8. (a) SEM cross-section image of AgNPs loaded on Si(111) substrate by immersing the substrate in solution I for 1 min;
3 (b) Typical cross-sectional SEM image of SiNW array on Si(111) substrate deposited with AgNPs after 30 min of etching in
4 HF/H_2O_2 with metallization aqueous solution I; (c) The L/R ratio of AgNPs randomly collected from ten sites at Fig (a) and (b).
5 (d) Enlarged cross-sectional image of the bottom of the arrays. Inset is the EDS spectrum of SiNWs recorded along the line.

6 In order to verify the mechanism, the evolution of Ag shape during the etching process was investigated,
7 and the results are shown in figure 8. Figure 8(b) shows some AgNPs locate at the bottom of the SiNW array.
8 The statistical analysis of L/R ratio of AgNPs randomly collected on Si(111) starting substrate and at the
9 bottom of the SiNW array is shown in figure 8(c). The average L/R aspect ratio of AgNPs at the bottom of
10 SiNWs array is larger than that on the starting wafers. In addition, many tiny and sparse nanoparticles appear
11 on the sidewalls of SiNWs, which is shown in figure 8(d). EDS spectrum of SiNWs recorded along the lines
12 is shown in the inset of figure 8(d), which confirms that the Ag nanoparticles indeed formed on the sidewalls
13 of SiNWs. Therefore, the afore-mentioned results agree to the proposed mechanism.

14 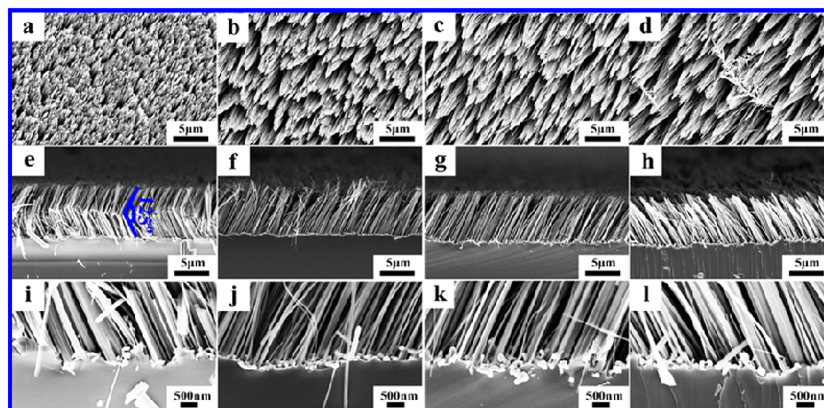

15 Figure 9. Images of SiNW arrays on n-type Si(110) substrate:(a), (b), (c), (d) planar image with no tilt angle; (e), (f), (g), (h)
16 cross section image; (i), (j), (k), (l) enlarged cross-sectional image of the bottom of the arrays. (a), (e), (i) in solution I; (b), (f), (j)
17 in solution II; (c), (g), (k) in solution III; (d), (h), (l) in solution IV.

CrystEngComm Accepted Manuscript

1 Similar phenomena of electrochemical etching occur in metal-assisted chemical etching of Si(110)
2 substrates with different shape of Ag catalyst. Figure 9 shows the SEM images of the as-obtained SiNW
3 arrays on Si(110) wafers etched in the aqueous solution of 0.7 M H_2O_2 and 4.8 M HF for the 30 min. The
4 large-area zigzag-shaped and slanting-aligned SiNW arrays on Si(110) substrates were obtained by depositing
5 AgNPs in different plating solutions. Figures 9(e) and (i) show SiNW arrays appearing uniform zigzag shape
6 with turning angle of 125° in the case of minimum L/R ratio of AgNPs. With further increasing the L/R ratio
7 of AgNPs, the etching direction switches to inclined direction, forming slantingly-aligned SiNW array as
8 shown in figure 9(f),(g) and (h).

9 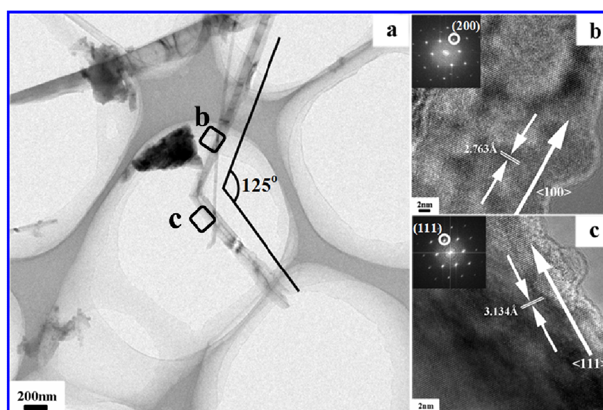

10 Figure 10. HRTEM characterizations of the single SiNW produced in metallization aqueous solution I for 30 min. (a)
11 Low-magnification image of the single zigzag-shaped SiNW. High-magnification bright-field images of the zigzag-shaped
12 SiNW (b) above and (c) below at transition. The insets show the corresponding Fast Fourier transform (FFT) patterns of the
13 HRTEM images shown in (b) and (c).

14 Figure 10 shows the TEM and HRTEM images of an individual zigzag-shaped SiNW. Two components
15 of single zigzag-shaped SiNW are tilted from each other by 125°, as labeled in figure 10(a). Figure 10(b) and
16 (c) are HRTEM images taken from the bright-field areas marked in figure 10(a). The HRTEM images
17 indicate that both segments of the zigzag-shaped SiNW are of single crystal. The lattice fringe spaces are
18 measured to 2.763 Å and 3.134 Å, which are in good agreement with (100) and (111) planes of crystalline Si,
19 respectively. From the corresponding FFT patterns of the HRTEM images, the directions of etching are also
20 confirmed to <100> and <111> for the components of single zigzag-shaped SiNW shown in figure 10(b) and

CrystEngComm Accepted Manuscript

1 figure 10(c), respectively. It can be calculated that the etching direction has initially <111> orientation incline
2 to the original substrate surface and switches into <100> orientation, leaving large-scale zigzag-shaped
3 SiNWs with 125° turning angle.

4
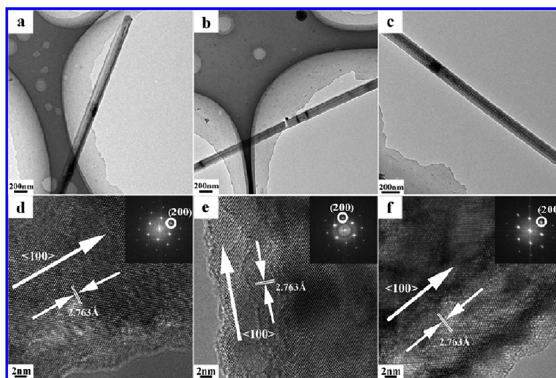

5 Figure 11. TEM and HRTEM images of single SiNW produced in different metallization aqueous solution at room
6 temperature for 30 min: (a), (d)in solution II; (b), (e) in solution III; (c), (f) in solution IV.

7 Typical TEM and HRTEM images of the as-obtained single SiNW produced on n-type Si(110) wafer
8 with different Ag nanostructures for 30 min are presented in figure 11. The well-resolved fringes and
9 corresponding FFT pattern are shown in the insets of figure 11(d), (e) and (f), which clearly indicate that both
10 of them are of single crystal. The lattice fringe spaces in figures 11(d,e,f) are 2.763 Å, which is in good
11 agreement with the inter-planar distance of (100) planes of crystalline Si. Therefore, with the increasing L/R
12 ratio of catalysts, the lateral etching becomes dominant and the etching direction has initially the lowest
13 energy of <100> direction.

14
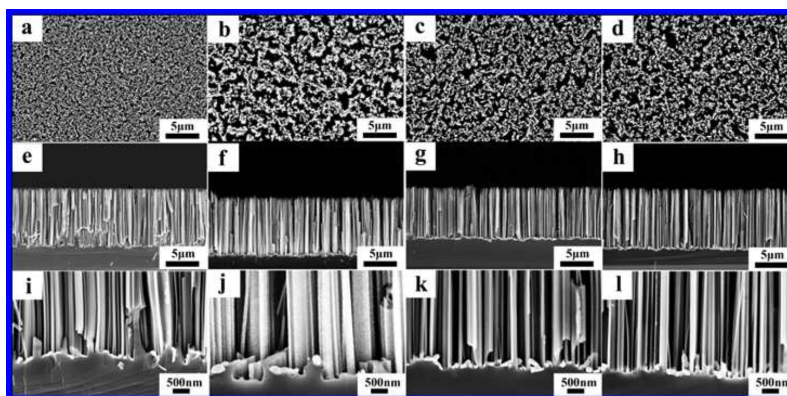

15 Figure 12.Images of SiNW arrays on n-type Si(100) substrate:(a), (b), (c), (d) planar image with no tilt angle; (e), (f), (g), (h)
16 cross section image; (i), (j), (k), (l) enlarged cross-sectional image of the bottom of the arrays. (a), (e), (i) in solution I; (b), (f), (j)
17 in solution II; (c), (g), (k) in solution III; (d), (h), (l) in solution IV.

CrystEngComm Accepted Manuscript

Electrochemical etching behavior is well-known to occur isotropically along <100> direction in metal-assisted chemical etching of the Si(100) wafer. Figure 12 shows the vertically-aligned SiNW arrays perpendicular to the Si(100) substrate with a length of about 10 μm, which was prepared in different metallization aqueous solution of $AgNO_3$ for 30 min. The continued etching in the vertical direction and formation of large area aligned SiNW arrays are perpendicular to the Si(100) substrate in despite of the different L/R ratio of AgNPs. The above experimental results can be interpreted by our proposed mechanism that the initially longitudinal etching direction is already the lowest energy of <100> direction. Therefore, the etching direction does not depend on the shape of the deposited metal catalyst and maintains in <100> direction during the whole etching process.

The above results indicated that the shape of the deposited metal catalyst has an important influence on the direction of anisotropy etching of Si(111) and Si(110) wafers. For larger L/R ratio of metal catalyst, etching process will be the integration of longitudinal and lateral etching and the etching direction will finally be fixed in <100> direction. We also found that the etching direction in isotropy etching of Si(100) does not depend on the shape of metal catalyst.

IV. CONCLUSIONS

In summary, we have investigated the anisotropic and isotropic etching behavior of SiNWs manufactured by MACE with different shape of Ag catalysts. The <100> is the preferred etching orientation and no lateral etching was observed in the etching of the (100) substrate. The etching directions of Si(111) and Si(110) are influenced by the L/R ratio of Ag catalysts. Assisted by minimum L/R ratio of AgNPs, the dominant etching direction is in longitudinal orientation. On the other hand, the etching process will be the integration of longitudinal and lateral etching as the average L/R ratio of catalysts increases. On the basis of

CrystEngComm Accepted Manuscript

1 these phenomena, a tentative mechanism has been developed to explain that the diameter-length ratio of 2 catalyst is an important factor affecting the etching orientation. According to the proposal mechanism, 3 longitudinal and lateral etching will be coexist in chemical anisotropy etching of Si(111) and Si(110) wafers, 4 especially in the case of larger L/R ratio of metal catalyst. On the other hand, the lateral etching in isotropy 5 etching of Si(100) can be ignored because initially longitudinal etching direction is already the lowest energy 6 of <100> direction.

7 ACKNOWLEDGMENTS

8 We gratefully acknowledge the nancial support for this work from Yangzhou Science and Technology 9 Development (No.YZ2011150) and Natural Science Foundation of Education Bureau of Jiangsu Province, 10 China (Grant No. 12KJB140012). we would also like to acknowledge the technical support received at the 11 Testing Center of Yangzhou University.

12

13

14

15

16

17

18

19

20

21

22

23

CrystEngComm Accepted Manuscript

1 # References

2 (1) Tian, B. Z.; Zheng, X. L.; Kempa, T. J.; Fang, Y.; Yu, N. F.; Yu, G. H.; Huang, J. L.; Lieber, C. M. Nature . 2007 , 449,
3 885-889.
4 (2) Garnett, E. C.; Yang, P. D. J. Am. Chem. Soc. 2008 , 130, 9224 -9225.
5 (3) Sivakov, V.; Andra, G.; Gawlik, A.; Berger, A.; Plentz, J.; Falk, F.;Christiansen, S. H. Nano Lett. 2009 , 9 , 1549-1554.
6 (4) Goldberger, J.; Hochbaum, A. I.; Fan, R.; Yang, P. Nano Lett.2006,6, 973-977.
7 (5) Schmidt, V.; Riel, H.; Senz, S.; Karg, S.; Riess, W. Small. 2006, 1, 85-88
8 (6) Chan, C. K.; Peng, H. L.; Liu, G.; McIlwrath, K.; Zhang, X. F.; Huggins, R. A.; Cui, Y. Nat. Nature Nanotechnology. 2008 ,
9 3,31-35.
10 (7) Zheng, G. F.; Patolsky, F.; Cui, Y.; Wang, W. U.; Lieber, C. M. Nat. Biotechnol. 2005 , 23 , 1294-1301.
11 (8) Yang ,Y. H.; Wu,S.J.; Chiu S.H.; Lin.P.; Chen Y.T. J. Phys. Chem. B. 2004,108, 846-852.
12 (9) Pan, H.; Lim. S.; Poh C.; Sun. H.; Wu. X.; Feng.Y.; Lin. J.; Nanotechnology. 2005, 16, 417-421.
13 (10) Lerose, D.; Bechelany, M.; Philippe, L.; Michler, J.; Christiansen, S. J. Cryst. Growth. 2010 , 312, 2887-2891.
14 (11) Huang, Z. P.; Fang, H.; Zhu, J. Adv. Mater. 2007,19, 744-748.
15 (12) Peng, K. Q.; Fang, H.; Hu, J. J.; Wu, Y.; Zhu, J.; Yan, Y. J.; Lee, S. T. Chem. Eur. J. 2006, 12 , 7942-7947.
16 (13) Qu, Y. Q.; Liao, L.; Li, Y. J.; Zhang, H.; Huang, Y.; Duan, X. F. Nano Lett. 2009 , 12, 4539-4543.
17 (14) Hochbaum, A. I.; Gargas, D.; Hwang, Y. J.; Yang, P. Nano Lett. 2009, 9, 3550–3554.
18 (15) Peng, K.; Hu, J.; Yan, Y.; Wu, Y.; Fang, H.; Xu, Y.; Lee, S. T.; Zhu, J. Adv. Funct. Mater. 2006, 16, 387–394.
19 (16) Peng, K.; Lu, A.; Zhang, R.; Lee, S.-T. Adv. Funct. Mater. 2008, 18, 3026–3035.
20 (17) Irrera, A.; Artoni, P.; Iacona, F.; Pecora, E. F.; Franzò, G.; Galli, M.; Fazio, B.; Priolo, F. Nanotechnology. 2012, 23,
21 075204-075211.
22 (18) Peng ,K. Q.; Yan, Y. J.; Gao, S. P.; Zhu, J. Adv Mater .2002, 14, 1164-1171.
23 (19) Buin, A. K.; Verma, A.; Svizhenko, A.; Anantram, M. P. Nano Lett. 2008, 8, 760-765.
24 (20) Hong, K. H.; Kim, J.; Lee, S. H.; Shin, J. K. Nano Lett. 2008, 8, 1335-1340.
25 (21) Fang, H.; Li, X. D.; Song, S.; Xu, Y.; Zhu, J. Nanotechnology 2008,19, 255703-255709 .
26 (22) Huang, Z. P.; Geyer. N.; Werner. P.; Gösele U. Adv. Mater. 2011, 23, 285–308.
27 (23) Huang, Z. P.; Shimizu, T.; Senz, S.; Zhang, Z.; Zhang, X. X.; Lee, W.; Geyer. N.; Gösele U. Nano Lett. 2009, 9,
28 2519-2525
29 (24) To, W. K.; Tsang, C. H.; Li, H. H.; Huang, Z. F. Nano Lett. 2011, 11, 5252-5258.
30 (25) Chang, S.W.; Chuang, V. P.; Boles, S. T.; Thompson, C. V.; Adv. Funct. Mater. 2010, 20, 4364–4370.

CrystEngComm Accepted Manuscript

1 (26) Huang, Z. P.; Shimizu, T.; Senz, S.; Zhang, Z.; Geyer, N.; Gösele U. J. Phys. Chem. C 2010, 114, 10683–10690.

2 (27) H. Chen.; H. Wang.; X. H. Zhang.; C. S. Lee.; S. T. Lee. Nano Lett. 2010, 10, 864-868.

3 (28) Peng, K.; Lu, A.; Zhang, R.; Lee, S. T. Adv. Funct. Mater. 2008,18, 3026-3035.

4 (29) Christophersen, M.; Cartensen, J.; Ronnebeck, S.; Jager, C.; Foll. H. J. Electrochem. Soc. 2001,148, 267-275.

5 (30) Morinaga, H.; Suyama, M.; Ohmi, T. J. Electrochem. Soc. 1994,141, 2834-2841.

6 (31) Xia, X. H.; Ashruf, C. M. A.; French, P. J.; Rappich, J.; Kelly, J. J. J. Phys. Chem. B 2001, 105, 5722-5729.

7 (32) Lehmann, V. J. Electrochem. Soc. 1993, 140, 2836-2843.

CrystEngComm Accepted Manuscript